Hyperfine Spectroscopy and Fast, All-Optical Arbitrary State Initialization and Readout of a Single, Ten-Level ^{73}Ge Vacancy Nuclear Spin Qudit in Diamond

C. Adambukulam,[1,*] B. C. Johnson,[2] A. Morello,[1] and A. Laucht[1,†]
[1]School of Electrical Engineering and Telecommunications, University of New South Wales, Kensington, NSW 2052, Australia
[2]School of Science, RMIT University, Melbourne, VIC 3001, Australia

(Received 11 September 2023; accepted 11 January 2024; published 9 February 2024)

A high-spin nucleus coupled to a color center can act as a long-lived memory qudit in a spin-photon interface. The germanium vacancy (GeV) in diamond has attracted recent attention due to its excellent spectral properties and provides access to the ten-dimensional Hilbert space of the $I = 9/2$ ^{73}Ge nucleus. Here, we observe the ^{73}GeV hyperfine structure, perform nuclear spin readout, and optically initialize the ^{73}Ge spin into any eigenstate on a μs timescale and with a fidelity of up to ∼84%. Our results establish ^{73}GeV as an optically addressable high-spin quantum platform for a high-efficiency spin-photon interface as well as for foundational quantum physics and metrology.

DOI: 10.1103/PhysRevLett.132.060603

Color centers are attractive candidates for light-matter qubit interfaces, as required to realize a quantum network [1–4]. In such systems, electrons bound to the color center potential provide a localized spin (or matter) qubit, while spin selective optical transitions enable spin initialization [5], readout [6], and spin-photon entanglement [3]. Group-IV split vacancy defects in diamond are particularly promising owing to their excellent spin [7,8] and spectral [6,9] properties, even when incorporated into nanostructures [10]. The group-IV defect of interest in this Letter, the germanium vacancy (GeV), has demonstrated an optical life and coherence time of $\tau_r \sim 5.9$ ns and $T^*_{2,\mathrm{opt}} \sim 9.5$ ns [6] in addition to electron spin coherence times exceeding ∼20 ms [11].

We can expand the quantum applications of color centers by including hyperfine coupled nuclear spins with coherence times that greatly exceed that of the electron [12]. For diamond-based color centers, work has typically focused on weakly coupled ^{13}C spins [13,14] with several fundamental demonstrations regarding quantum networks having been performed with them [15–18]. However, the nondeterministic inclusion of the ^{13}C isotope presents additional challenges with regards to locating ^{13}C nuclear spins. In contrast, each of the group-IV elements has at least one isotope with a nuclear spin. High cooperativity between a group-IV defect and a nanophotonic cavity allows for these intrinsic nuclear spins to serve as quantum memories, thereby bypassing the need to locate ^{13}C spins. This has been demonstrated for the ^{29}SiV [19].

Of all the group-IV isotopes, including ^{13}C, only ^{73}Ge has a high nuclear spin ($I > 1/2$). In fact, the $I = 9/2$ ^{73}Ge spin spans a ten-dimensional Hilbert space. Several proposed schemes [20–22] map a two-level qubit onto a nuclear spin qudit and leverage the redundancy of a large Hilbert space for error correction. Such schemes could significantly improve the storage time of a nuclear spin-based quantum memory. In addition, high-spin nuclei are a potential platform for investigating several fundamental questions in quantum mechanics; from quantum chaos [23] to the reality of the wave function [24], and as well as for quantum metrology, where spin analogs to nonclassical states [25] of light may improve sensor gain. However, the experimental study of solid-state high-spin nuclei has been limited, with few experimental platforms available [26–29]. This extends further when considering optically active defects as other centers with access to a high-spin nucleus [30–33] have either yet to demonstrate single defect optical addressability or do not exhibit comparable spin and spectral properties.

In this Letter, we experimentally establish the negatively charged ^{73}GeV in diamond as a powerful, optically addressable ten-level nuclear spin platform in the solid state. We perform coherent population trapping (CPT) experiments to resolve the hyperfine structure of the ^{73}GeV. Using pulsed CPT, we read out the nuclear spin state and observe rapid nuclear spin diffusion that arises from nuclear spin nonconserving optical relaxation. We leverage these relaxation processes to perform fast, high-fidelity all-optical initialization of the ^{73}Ge spin into any of its eigenstates.

Figure 1(a) shows the level structure of the ^{73}GeV where $|1\rangle$ and $|2\rangle$ refer to the electron spin-down and spin-up eigenstates of the ground state (GS) and $|A\rangle$ to the electron spin-down eigenstate of the optically excited state (ES). In an off-axis magnetic field, $B_0 \nparallel [111]$ [see Fig. 1(b)], the transition between $|2\rangle$ and $|A\rangle$ is weakly allowed, resulting

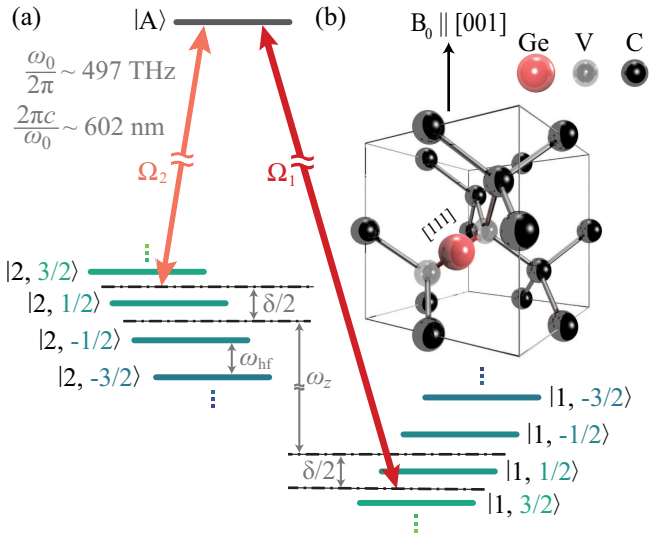

FIG. 1. (a) Level structure of the ^{73}GeV, with CPT driving lasers denoted by the orange and red arrows. The optical Rabi frequency between $|A\rangle$ and $|1\rangle$ and between $|A\rangle$ and $|2\rangle$ is Ω_1 and Ω_2. The lasers have frequencies approximately equal to the GeV zero-phonon line of $\omega_0/2\pi \sim 497$ THz or ~602 nm. Additionally, c, δ, ω_z, and ω_{hf} refer to the vacuum speed of light, two laser detuning, Zeeman splitting, and hyperfine splitting. (b) Diagram of the GeV with the orientation of the magnetic field, B_0, shown. The angle between B_0 and [111] is ~54.7°. Ge, V, and C refer to germanium, vacancy, and carbon, respectively.

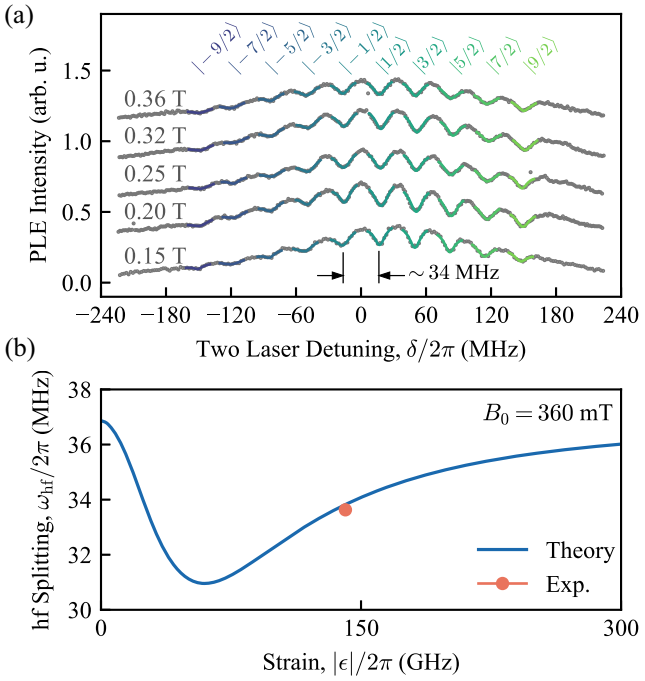

FIG. 2. (a) Coherent population trapping spectra with B_0 varied (gray text). The CPT power ranges from ~220 to ~420 nW or equivalently, between 3 and 6 times the saturation power of A1—which was measured to be $p_{sat} = 70 \pm 5$ nW. The data (gray dots) is fit (colored lines) to ten copies of a Lorentzian, $A/[1 + (\delta - \delta_0)/\gamma)^2] + C(\delta - \delta_0) + D$ [34]. Each copy is centered on a particular *dip* that corresponds to one of the ten nuclear spin eigenstates ordered $|-9/2\rangle$ to $|9/2\rangle$ from left to right. (b) Calculated strain dependence of the hyperfine splitting when $B_0 \| [001]$ and $A/2\pi = 36.98$ MHz. The orange point indicates the experimentally measured hyperfine splitting.

in a Λ system. We perform CPT [5,41–43] by applying two equal power (as imposed by the experimental setup [34]) lasers to simultaneously drive the $|1\rangle \leftrightarrow |A\rangle$ and $|2\rangle \leftrightarrow |A\rangle$ (denoted A1 and A2) transitions with Rabi frequencies Ω_1 and Ω_2 as shown in Fig. 1(a). In a system where no hyperfine coupled nuclear spin is present and when the two laser detuning, $\delta/2\pi = 0$ MHz [defined in Fig. 1(a) and Ref. [34]], the system steady state is the so-called "dark state"; a superposition of $|1\rangle$ and $|2\rangle$ that produces a *dip* in a photoluminescence excitation (PLE) spectrum [44]. A hyperfine coupled nuclear spin introduces a nuclear state dependent shift $\sim m\omega_{hf}$—for a nuclear state $|m\rangle$—to the CPT resonance such that it may no longer be at $\delta/2\pi = 0$ MHz. The Hamiltonian that describes this interaction is

$$H_{hf} = \frac{A_\perp}{2}(S_+ I_- + S_- I_+) + A_\parallel S_z I_z, \qquad (1)$$

where S_i (I_i) for $i \in \{x, y, z\}$ are the electron (nuclear) spin operators, $S_\pm = S_x \pm iS_y$ (and likewise, $I_\pm = I_x \pm iI_y$) and $A_\parallel$ ($A_\perp$) is the longitudinal (transverse) hyperfine coupling. As the GS wave function parity is even, the isotropic Fermi contact interaction dominates [5,45] and $A = A_\parallel \sim A_\perp$.

In Fig. 2(a), we plot the results of a CPT measurement on a single ^{73}GeV center. Note the single laser detuning and sample temperature is ~0 MHz and ~25 mK in this and all experiments described hereafter [34]. Furthermore, as shown in Fig. 1(a), we perform CPT by sweeping δ and changing frequency of both lasers. We observe ten B_0 independent dips, split by $\omega_{hf}/2\pi = 33.81 \pm 0.05$ MHz, that correspond to the ten ^{73}Ge spin eigenstates. As with the ^{29}SiV [46], ω_{hf} depends on the strain and B_0 orientation [see Fig. 2(b)]. By fitting the measured ω_{hf} to the GeV Hamiltonian, we extract $A_\parallel/2\pi = 36.98 \pm 0.06$ MHz assuming an orbital Zeeman effect of $\sim 0.1\gamma_e B_0/2$ GHz [47]. The measured value is in good agreement with its *ab initio* prediction in Ref. [45]. The strain dependence of ω_{hf} arises from strain induced mixing of the electron spin and orbital degrees of freedom (see Ref. [34]) that occurs when strain, $|\epsilon|$ is comparable to the spin-orbit coupling, $\lambda \sim$ 165 GHz [48]. At low excitation powers, the CPT *dip* width is given by $\propto T_2^{*-1}$. In practice, we choose excitation powers such that, $\Omega_1, \Omega_2 \gg T_2^{*-1}$ to ensure *dip* visibility [42]. This lowers the CPT resolution by way of power broadening (from several 100 kHz to several MHz) and thus, we cannot measure the ~kHz [45] magnitude shifts produced by the second order hyperfine and quadrupole interactions.

We apply perturbation theory to the ^{73}GeV hyperfine structure (see Ref. [34]) to understand its strain dependence.

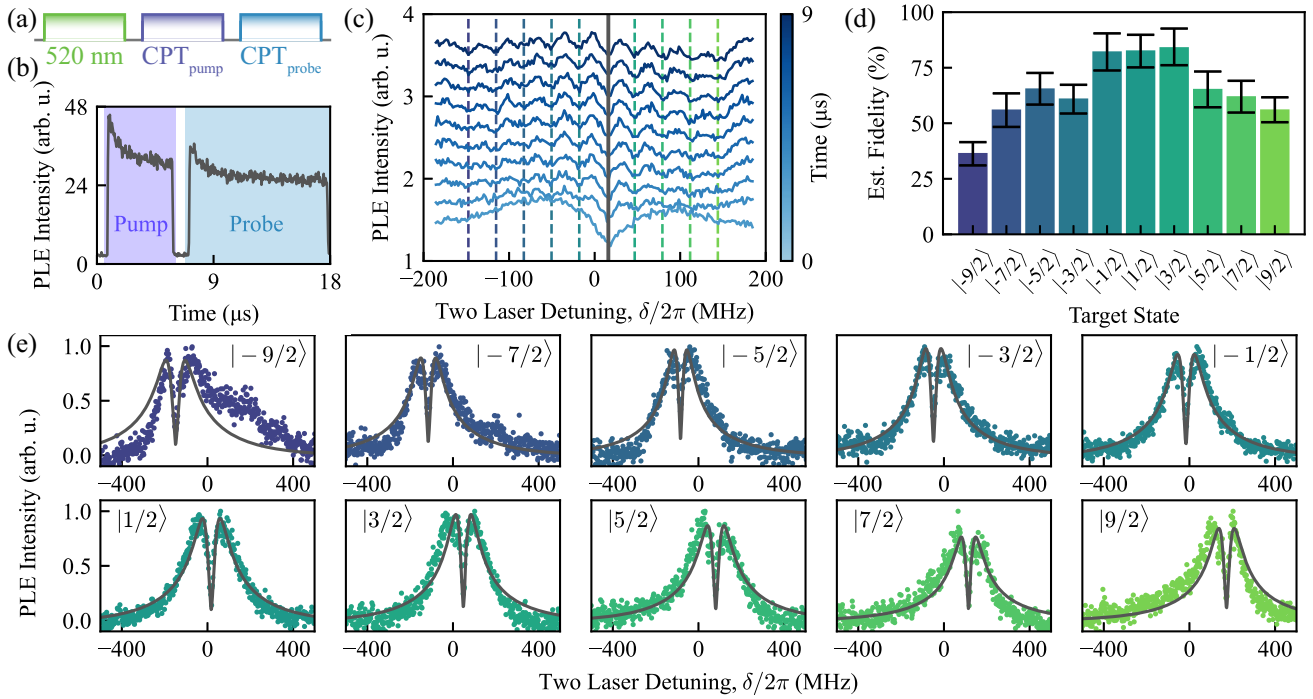

FIG. 3. (a) Pulse sequence for a nuclear pump-probe experiment. $\mathrm{CPT}_{\mathrm{pump}}$ and $\mathrm{CPT}_{\mathrm{probe}}$ refer to two CPT pulses—each pulse consisting of two simultaneously applied lasers—where δ is either fixed and resonant to a CPT *dip* (pump) or varied during the experiment (probe). Note, *pump* and *probe* exclusively refer to the effect of these pulses on the nuclear spin. (b) A histogram of the photon arrival times measured during a nuclear pump-probe experiment. $\mathrm{CPT}_{\mathrm{pump}}$ is resonant to $|1/2\rangle$ while $\mathrm{CPT}_{\mathrm{probe}}$ is resonant to $|5/2\rangle$. (c) Time resolved PLE intensity during a probe pulse. The $\mathrm{CPT}_{\mathrm{pump}}$ pulse is resonant to $|1/2\rangle$ as denoted by the solid gray line. The dashed colored lines indicate the resonances of the other nuclear spin eigenstates. (d) The estimated initialization fidelity achieved for each nuclear spin eigenstate. Here, the error bars refer to the 95% confidence interval. (e) CPT spectra measured by the nuclear pump-probe technique with the PLE intensity measured during the first 250 ns of the $\mathrm{CPT}_{\mathrm{probe}}$ pulse. The data (colored dots) have been fit to the steady state of a CPT Lindbladian (gray lines; see Ref. [34]). The $\mathrm{CPT}_{\mathrm{pump}}$ frequency is indicated by the color of the dots, which corresponds to the color of dashed lines in (c) with the associated nuclear spin state labeled adjacent to the data (gray text).

We find that the impact of strain on the effective transverse hyperfine coupling is analogous to its impact on the electron g factor [34,47,49]. More explicitly, and up to the second order in ϵ, $A_{\perp}^{\mathrm{eff}} = 4|\epsilon|A_{\perp}/\lambda$. Given that the nuclear Zeeman effect is weak, the hyperfine interaction entirely dominates the dynamics of the nuclear spin.

We perform a pump-probe experiment with the pulse sequence shown in Fig. 3(a). We apply a CPT-pump pulse where δ is resonant with a particular nuclear state, followed by a CPT-probe pulse where δ is varied for nuclear spin readout [50]. The ~520 nm pulse stabilizes the GeV charge state [51]. The time resolved PLE, collected during the probe pulse, is shown in the histograms in Figs. 3(b) and 3(c). In Fig. 3(c), this is done with the pump-pulse resonant with the nuclear spin eigenstate, $|1/2\rangle$. The PLE measured at the start of the probe pulse then verifies that the nuclear spin was pumped into $|1/2\rangle$. This is extended to the entire nuclear spin Hilbert space as shown in Fig. 3(e) where the different panels show initialization into all ten nuclear spin eigenstates. The estimated initialization fidelities for each eigenstate are plotted in Fig. 3(d) and are computed from the data in Fig. 3(e). We estimate typical fidelities of ~65% with the highest fidelity of $84^{+9}_{-8}\%$ deduced for $|3/2\rangle$.

The initialization mechanism is as follows: at the start of a target-state-resonant CPT pulse, the nuclear spin is in an arbitrary state and thus, the CPT pulse is not resonant with the system. Consequently, optical excitation occurs and the subsequent relaxation flips the nuclear spin. The nuclear spin continues to flip, or diffuse, until it reaches the target state upon which formation of the CPT dark state terminates the process. This protocol has found applications in Overhauser field cooling of self-assembled quantum dots [52] and nitrogen vacancy centers [53]. In those systems, nuclear spin diffusion arises from the transverse hyperfine interaction, $A_{\perp}(S_{+}I_{-} + S_{-}I_{+})$, which generates electron-nuclear spin flip-flops. For highly strained group-IV defects, ω_z suppresses this term [54] resulting in nuclear spin raising and lowering rates of $A_{\perp}^2\Gamma_r/4\omega_z^2$ and $A_{\perp}^2\Gamma_r/4\eta\omega_z^2 \sim 10$–$100$ Hz. Here, Γ_r is the optical relaxation rate and $\eta \approx \Omega_1^2/\Omega_2^2$ is the branching ratio. In Fig. 4(c), we plot the relationship between dark-state formation rate and laser power during the nuclear spin initialization protocol. To measure this, we modify the

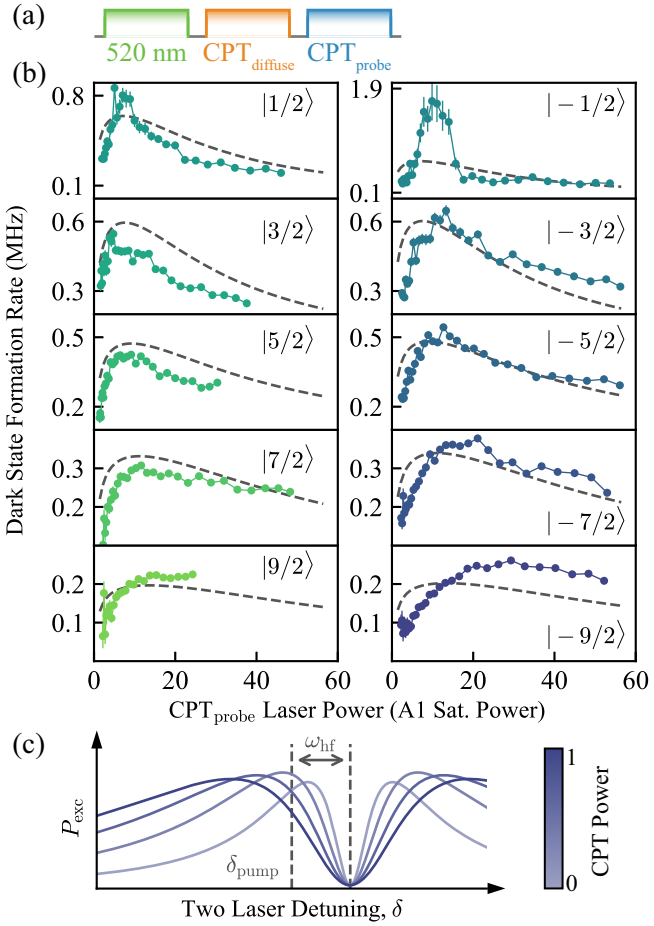

FIG. 4. Nuclear spin initialization time. (a) The pulse sequence used to measure the nuclear spin initialization time. Here, $\mathrm{CPT}_{\mathrm{diffuse}}$ refers to a completely off-resonant, $\delta = 0$ MHz CPT pulse. (b) The power dependence of the nuclear spin initialization rates for each nuclear spin eigenstate. Here, the laser power is expressed in terms of the A1 saturation power, $p_{\mathrm{sat}} = 70 \pm 5$ nW. The colored points denote the measured data while the gray dashed lines plot the theoretical initialization rate extracted from a rate model. (c) Schematic diagram of the excitation probability, P_{exc}, at the beginning of a $\mathrm{CPT}_{\mathrm{pump}}/\mathrm{CPT}_{\mathrm{probe}}$ pulse. Here, δ is set to pump the nuclear spin eigenstate adjacent to the initial state of the system resulting in a CPT detuning of ω_{hf} from the resonance. Note, when the CPT power is large, increasing it further reduces the excitation rate as the *dip* broadens and consequently suppresses nuclear spin diffusion.

nuclear pump-probe pulse sequence [see Fig. 3(a)] to a diffuse-probe sequence [see Fig. 4(b)] wherein the two laser detuning of the first pulse is $\delta/2\pi = 0$ MHz and completely off-resonant to any nuclear spin eigenstate. This pumps the nuclear spin into a mixed state from which we may initialize a specific nuclear spin projection. By fixing δ during the CPT-diffuse pulse, the state populations of the resulting mixed state are the same between the various experimental runs. We measure initialization rates exceeding 100 kHz for all ten eigenstates, which is far beyond what the transverse hyperfine could produce.

We extend our perturbative model of the ^{73}GeV hyperfine structure to its dipole operators [34]. We find that the difference in GS and ES strain modulates the nuclear spin flipping transition strength. This is analogous to the electron spin flipping transition, A2, its intensity being strain modulated. The largest contribution to nuclear spin diffusion is the difference in the GS and ES nuclear spin quantization axes. As the hyperfine interaction dominates, the nuclear spin quantization direction depends on that of the electron and on the components of the hyperfine tensor. Whereas the GS hyperfine tensor is dominated by the isotropic Fermi contact interaction, the ES hyperfine tensor is expected to be dominated by the anisotropic dipolar term [55]. This, in combination with differing GS and ES g tensors results in different GS and ES nuclear spin quantization axes, thereby increasing the likelihood of relaxation induced nuclear spin flips.

We construct a rate model of the nuclear spin pumping process [34], to gain insight into its excitation power dependence [see Fig. 4(a)]. In particular, we note that rather than saturating, the pumping rate decreases after some optimum power. This is a consequence of power broadening [see Fig. 4(c)]. Wider CPT dips suppress optical excitation and slow the nuclear spin diffusion process. Deviation of the rate model from the experiment is due to sensitivity of the modeled nuclear spin quantization axis to the unknown value of the ES hyperfine and in addition to errors and fluctuations in δ for both CPT pulses in the several hours of averaging required to perform the experiment.

Given the nuclear spin diffusion during the probe pulse [see Fig. 3(c), where the remaining nine *dips* appear after the CPT-probe pulse is applied for several μs], the fidelity estimates shown in Fig. 3(d) are conservative. Additionally, PLE intensity drift during the measurement further limits the accuracy of fidelity estimation. The low initialization fidelity into $|-9/2\rangle$ is likely due to the difficulty in ascertaining the corresponding δ given its low CPT contrast and in addition to fast nuclear spin diffusion away from $|-9/2\rangle$ during the CPT-probe pulse. Fidelity is limited by errors in δ—an effect amplified by power broadening. The fundamental limit to fidelity is the probability of re-excitation from the dark state, given by the ratio of the optical lifetime and the electron T_2^* [34]. The initialization fidelity stands to be improved through the optimization of T_2^* by isotopic purification of the diamond and by aligning B_0 to [111] [7,11] while minimizing errors in δ.

CPT-based nuclear spin pumping [56] provides access to nuclear spin systems where the difference between the GS and ES hyperfine splittings does not exceed the optical linewidth [57] and presents less overhead than traditional initialization schemes such as electron initialization followed by a SWAP gate [19], dynamic nuclear polarization [58], or measurement-based initialization [59]. Moreover, the ability to polarize into any nuclear eigenstate

allows one to bypass rf control of the nuclear spin during initialization. This is highly desirable given the large, ten-dimensional nuclear spin Hilbert space and the low ^{73}Ge gyromagnetic ratio, $\gamma_n \sim 1.5$ MHz/T. For example, assuming a high rf power to magnetic field conversion efficiency as achieved in Ref. [60] and a dilution refrigerator power budget of 100 μW, we would expect nuclear Rabi frequencies on the order of ∼100 Hz and significantly lower initialization rates. In contrast, we show μs-timescale initialization rates comparable to that of the electron spin (see Ref. [34]). On the other hand, the fast nuclear spin diffusion makes nuclear spin readout with CPT difficult, as the number of collected photons per shot is $\ll 1$. However, we expect that the nuclear spin diffusion rate may be lowered by aligning B_0 with the defect axis and, in doing so, improve CPT-based nuclear spin readout. Additionally, alternative readout mechanisms exist. Namely, a nuclear spin conditional operation on the electron and its subsequent readout [19,61], which may also enable single-shot nuclear spin readout.

The long coherence times of solid-state nuclear spins [12] make them an invaluable resource for color-center-based spin-photon interfaces, which has motivated recent investigations into the intrinsic nuclear spins of group-IV defects [19,55,57]. In this Letter, we observe the hyperfine structure of the ^{73}GeV and measure $A_{\parallel} \sim 37$ MHz. Furthermore, we demonstrate optical readout and initialization of the ^{73}Ge spin, quickly and without requiring microwave or rf magnetic fields. This constitutes a feature that significantly improves the feasibility of addressing the nuclear spin, given its large Hilbert space and low gyromagnetic ratio. Our work will fundamentally enable a near-term demonstration of coherent control of the ^{73}Ge spin, either via all-optical [62] or magnetic methods. In the long term, the ^{73}GeV system could be deployed as an optically accessible qudit for quantum information processing [63], as a platform to explore quantum chaos [23], or to generate nonclassical spin states of metrological interest [25].

We would like to thank Blake Regan for his assistance with sample preparation and Hyma H. Vallabhapurapu for useful discussions. We acknowledge funding from the Australian Research Council (Grant No. CE170100012). This work used the facilities of the Australian National Fabrication Facility (ANFF). We acknowledge access and support to NCRIS facilities (ANFF and the Heavy Ion Accelerator Capability) at the Australian National University. C. A. and A. L. acknowledge support from the University of New South Wales Scientia program.

*Corresponding author: c.adambukulam@unsw.edu.au
†a.laucht@unsw.edu.au

[1] M. Ruf, N. H. Wan, H. Choi, D. Englund, and R. Hanson, Quantum networks based on color centers in diamond, J. Appl. Phys. **130**, 070901 (2021).
[2] E. Togan, Y. Chu, A. S. Trifonov, L. Jiang, J. Maze, L. Childress, M. V. G. Dutt, A. S. Sørensen, P. R. Hemmer, A. S. Zibrov, and M. D. Lukin, Quantum entanglement between an optical photon and a solid-state spin qubit, Nature (London) **466**, 730 (2010).
[3] C. T. Nguyen, D. D. Sukachev, M. K. Bhaskar, B. Machielse, D. S. Levonian, E. N. Knall, P. Stroganov, R. Riedinger, H. Park, M. Lončar, and M. D. Lukin, Quantum network nodes based on diamond qubits with an efficient nanophotonic interface, Phys. Rev. Lett. **123**, 183602 (2019).
[4] B. Hensen, H. Bernien, A. E. Dréau, A. Reiserer, N. Kalb, M. S. Blok, J. Ruitenberg, R. F. L. Vermeulen, R. N. Schouten, C. Abellán, W. Amaya, V. Pruneri, M. W. Mitchell, M. Markham, D. J. Twitchen, D. Elkouss, S. Wehner, T. H. Taminiau, and R. Hanson, Loophole free bell inequality violation using electron spins separated by 1.3 kilometres, Nature (London) **526**, 682 (2015).
[5] L. J. Rogers, K. D. Jahnke, M. H. Metsch, A. Sipahigil, J. M. Binder, T. Teraji, H. Sumiya, J. Isoya, M. D. Lukin, P. Hemmer, and F. Jelezko, All-optical initialization, readout, and coherent preparation of single silicon vacancy spins in diamond, Phys. Rev. Lett. **113**, 263602 (2014).
[6] D. Chen, J. E. Fröch, S. Ru, H. Cai, N. Wang, G. Adamo, J. Scott, F. Li, N. Zheludev, I. Aharonovich, and W. Gao, Quantum interference of resonance fluorescence from germanium-vacancy color centers in diamond, Nano Lett. **22**, 6306 (2022).
[7] D. D. Sukachev, A. Sipahigil, C. T. Nguyen, M. K. Bhaskar, R. E. Evans, F. Jelezko, and M. D. Lukin, Silicon-vacancy spin qubit in diamond: A quantum memory exceeding 10 ms with single-shot state readout, Phys. Rev. Lett. **119**, 223602 (2017).
[8] R. Debroux, C. P. Michaels, C. M. Purser, N. Wan, M. E. Trusheim, J. Arjona Martínez, R. A. Parker, A. M. Stramma, K. C. Chen, L. de Santis, E. M. Alexeev, A. C. Ferrari, D. Englund, D. A. Gangloff, and M. Atatüre, Quantum control of the tin-vacancy spin qubit in diamond, Phys. Rev. X **11**, 041041 (2021).
[9] L. J. Rogers, K. D. Jahnke, T. Teraji, L. Marseglia, C. Müller, B. Naydenov, H. Schauffert, C. Kranz, J. Isoya, L. P. McGuinness, and F. Jelezko, Multiple intrinsically identical single-photon emitters in the solid state, Nat. Commun. **5**, 4739 (2014).
[10] M. E. Trusheim *et al.*, Transform limited photons from a coherent tin-vacancy spin in diamond, Phys. Rev. Lett. **124**, 023602 (2020).
[11] K. Senkalla, G. Genov, M. H. Metsch, P. Siyushev, and F. Jelezko, Germanium vacancy in diamond quantum memory exceeding 20 ms, arXiv:2308.09666.
[12] G. Waldherr, J. Beck, P. Neumann, R. S. Said, M. Nitsche, M. L. Markham, D. J. Twitchen, J. Twamley, F. Jelezko, and J. Wrachtrup, High-dynamic-range magnetometry with a single nuclear spin in diamond, Nat. Nanotechnol. **7**, 105 (2012).
[13] M. V. G. Dutt, L. Childress, L. Jiang, E. Togan, J. Maze, F. Jelezko, A. S. Zibrov, P. R. Hemmer, and M. D. Lukin,

Quantum register based on individual electronic and nuclear spin qubits in diamond, Science **316**, 1312 (2007).
[14] C. E. Bradley, J. Randall, M. H. Abobeih, R. C. Berrevoets, M. J. Degen, M. A. Bakker, M. Markham, D. J. Twitchen, and T. H. Taminiau, A ten-qubit solid state spin register with quantum memory up to one minute, Phys. Rev. X **9**, 031045 (2019).
[15] N. Kalb, A. A. Reiserer, P. C. Humphreys, J. J. W. Bakermans, S. J. Kamerling, N. H. Nickerson, S. C. Benjamin, D. J. Twitchen, M. Markham, and R. Hanson, Entanglement distillation between solid-state quantum network nodes, , Science **356**, 928 (2017).
[16] K. Tsurumoto, R. Kuroiwa, H. Kano, Y. Sekiguchi, and H. Kosaka, Quantum teleportation-based state transfer of photon polarization into a carbon spin in diamond, Commun. Phys. **2**, 74 (2019).
[17] M. Pompili, S. L. N. Hermans, S. Baier, H. K. C. Beukers, P. C. Humphreys, R. N. Schouten, R. F. L. Vermeulen, M. J. Tiggelman, L. dos Santos Martins, B. Dirkse, S. Wehner, and R. Hanson, Realization of a multinode quantum network of remote solid-state qubits, Science **372**, 259 (2021).
[18] S. L. N. Hermans, M. Pompili, H. K. C. Beukers, S. Baier, J. Borregaard, and R. Hanson, Qubit teleportation between non-neighbouring nodes in a quantum network, Nature (London) **605**, 663 (2022).
[19] P.-J. Stas, Y. Q. Huan, B. Machielse, E. N. Knall, A. Suleymanzade, B. Pingault, M. Sutula, S. W. Ding, C. M. Knaut, D. R. Assumpcao, Y.-C. Wei, M. K. Bhaskar, R. Riedinger, D. D. Sukachev, H. Park, M. Lončar, D. S. Levonian, and M. D. Lukin, Robust multi-qubit quantum network node with integrated error detection, Science **378**, 557 (2022).
[20] J. A. Gross, C. Godfrin, A. Blais, and E. Dupont-Ferrier, Hardware-efficient error-correcting codes for large nuclear spins, arXiv:2103.08548.
[21] F. Petiziol, A. Chiesa, S. Wimberger, P. Santini, and S. Carretta, Counteracting dephasing in molecular nanomagnets by optimized qudit encodings, npj Quantum Inf. **7**, 133 (2021).
[22] J. A. Gross, Designing codes around interactions: The case of a spin, Phys. Rev. Lett. **127**, 010504 (2021).
[23] V. Mourik, S. Asaad, H. Firgau, J. J. Pla, C. Holmes, G. J. Milburn, J. C. McCallum, and A. Morello, Exploring quantum chaos with a single nuclear spin, Phys. Rev. E **98**, 042206 (2018).
[24] J. Barrett, E. G. Cavalcanti, R. Lal, and O. J. E. Maroney, No ψ-epistemic model can fully explain the indistinguishability of quantum states, Phys. Rev. Lett. **112**, 250403 (2014).
[25] Y. Aksu Korkmaz and C. Bulutay, Nuclear spin squeezing via electric quadrupole interaction, Phys. Rev. A **93**, 013812 (2016).
[26] S. Asaad, V. Mourik, B. Joecker, M. A. I. Johnson, A. D. Baczewski, H. R. Firgau, M. T. Mądzik, V. Schmitt, J. J. Pla, F. E. Hudson *et al.*, Coherent electrical control of a single high-spin nucleus in silicon, Nature (London) **579**, 205 (2020).
[27] E. A. Chekhovich, S. F. C. da Silva, and A. Rastelli, Nuclear spin quantum register in an optically active semiconductor quantum dot, Nat. Nanotechnol. **15**, 999 (2020).
[28] S. Thiele, F. Balestro, R. Ballou, S. Klyatskaya, M. Ruben, and W. Wernsdorfer, Electrically driven nuclear spin resonance in single-molecule magnets, Science **344**, 1135 (2014).
[29] I. F. de Fuentes, T. Botzem, M. A. I. Johnson, A. Vaartjes, S. Asaad, V. Mourik, F. E. Hudson, K. M. Itoh, B. C. Johnson, A. M. Jakob, J. C. McCallum, D. N. Jamieson, A. S. Dzurak, and A. Morello, Navigating the 16-dimensional Hilbert space of a high-spin donor qudit with electric and magnetic fields, arXiv:2306.07453.
[30] J. Hendriks, C. M. Gilardoni, C. Adambukulam, A. Laucht, and C. H. van der Wal, Coherent spin dynamics of hyperfine-coupled vanadium impurities in silicon carbide, arXiv:2210.09942.
[31] T. Bosma, G. J. J. Lof, C. M. Gilardoni, O. V. Zwier, F. Hendriks, B. Magnusson, A. Ellison, A. Gällström, I. G. Ivanov, N. T. Son, R. W. A. Havenith, and C. H. van der Wal, Identification and tunable optical coherent control of transition-metal spins in silicon carbide, npj Quantum Inf. **4**, 48 (2018).
[32] J. Yang, W. Fan, Y. Zhang, C. Duan, G. G. de Boo, R. L. Ahlefeldt, J. J. Longdell, B. C. Johnson, J. C. McCallum, M. J. Sellars, S. Rogge, C. Yin, and J. Du, Zeeman and hyperfine interactions of a single $^{127}Er^{3+}$ ion in Si, Phys. Rev. B **105**, 235306 (2022).
[33] M. L. K. Viitaniemi, C. Zimmermann, V. Niaouris, S. H. D'Ambrosia, X. Wang, E. S. Kumar, F. Mohammadbeigi, S. P. Watkins, and K.-M. C. Fu, Coherent spin preparation of indium donor qubits in single ZnO nanowires, Nano Lett. **22**, 2134 (2022).
[34] See Supplemental Material at http://link.aps.org/supplemental/10.1103/PhysRevLett.132.060603, which includes Refs. [35–40], for details regarding the sample preparation, experimental setup, perturbative modeling of the GeV and its hyperfine structure, and rate modeling of nuclear spin diffusion and nuclear spin lifetime.
[35] I. Shavitt and L. T. Redmon, Quasidegenerate perturbation theories. A canonical van Vleck formalism and its relationship to other approaches, J. Chem. Phys. **73**, 5711 (2008).
[36] S. Maity, B. Pingault, G. Joe, M. Chalupnik, D. Assumpçao, E. Cornell, L. Shao, and M. Lončar, Mechanical control of a single nuclear spin, Phys. Rev. X **12**, 011056 (2022).
[37] P. Rungta, V. Bužek, C. M. Caves, M. Hillery, and G. J. Milburn, Universal state inversion and concurrence in arbitrary dimensions, Phys. Rev. A **64**, 042315 (2001).
[38] D. Manzano, A short introduction to the Lindblad master equation, AIP Adv. **10**, 025106 (2020).
[39] C. Adambukulam, J. A. Scott, S. Q. Lim, I. Aharonovich, A. Morello, and A. Laucht, Coherent all-optical control of a solid-state spin via a double Λ-system, arXiv:2402.00244.
[40] S. G. Carter, S. C. Badescu, A. S. Bracker, M. K. Yakes, K. X. Tran, J. Q. Grim, and D. Gammon, Coherent population trapping combined with cycling transitions for quantum dot hole spins using triplet trion states, Phys. Rev. Lett. **126**, 107401 (2021).
[41] B. Pingault, J. N. Becker, C. H. H. Schulte, C. Arend, C. Hepp, T. Godde, A. I. Tartakovskii, M. Markham, C. Becher, and M. Atatüre, All-optical formation of coherent dark states of silicon-vacancy spins in diamond, Phys. Rev. Lett. **113**, 263601 (2014).

[42] B. D. Agap'ev, M. B. Gornyĭ, B. Matisov, and Y. V. Rozhdestvenskiĭ, Coherent population trapping in quantum systems, Phys. Usp. **36**, 763 (1993).
[43] X. Xu, S. Bo, P. R. Berman, D. G. Steel, A. S. Bracker, D. Gammon, and L. Sham, Coherent population trapping of an electron spin in a single negatively charged quantum dot, Nat. Phys. **4**, 692 (2008).
[44] E. Arimondo, in *Progress in Optics* (Elsevier, New York, 1996), Vol. 35, pp. 257–354.
[45] A. Karim, H. H. Vallabhapurapu, C. Adambukulam, A. Laucht, S. P. Russo, and A. Peruzzo, All-electron ab-initio hyperfine coupling of Si-, Ge- and Sn -vacancy defects in diamond, arXiv:2309.13913.
[46] B. Pingault, D.-D. Jarausch, C. Hepp, L. Klintberg, J. N. Becker, M. Markham, C. Becher, and M. Atatüre, Coherent control of the silicon-vacancy spin in diamond, Nat. Commun. **8**, 15579 (2017).
[47] C. Hepp, T. Müller, V. Waselowski, J. N. Becker, B. Pingault, H. Sternschulte, D. Steinmüller-Nethl, A. Gali, J. R. Maze, M. Atatüre, and C. Becher, Electronic structure of the silicon vacancy color center in diamond, Phys. Rev. Lett. **112**, 036405 (2014).
[48] S. Maity, L. Shao, Y.-I. Sohn, S. Meesala, B. Machielse, E. Bielejec, M. Markham, and M. Lončar, Spectral alignment of single-photon emitters in diamond using strain gradient, Phys. Rev. Appl. **10**, 024050 (2018).
[49] C. J. Hepp, Electronic structure of the silicon vacancy color center in diamond, Ph.D. thesis, Universität des Saarlandes, 2014.
[50] D. A. Golter, K. N. Dinyari, and H. Wang, Nuclear-spin-dependent coherent population trapping of single nitrogen-vacancy centers in diamond, Phys. Rev. A **87**, 035801 (2013).
[51] D. Chen, Z. Mu, Y. Zhou, J. E. Fröch, A. Rasmit, C. Diederichs, N. Zheludev, I. Aharonovich, and W. B. Gao, Optical gating of resonance fluorescence from a single germanium vacancy color center in diamond, Phys. Rev. Lett. **123**, 033602 (2019).
[52] G. Éthier-Majcher, D. Gangloff, R. Stockill, E. Clarke, M. Hugues, C. Le Gall, and M. Atatüre, Improving a solid-state qubit through an engineered mesoscopic environment, Phys. Rev. Lett. **119**, 130503 (2017).
[53] E. Togan, Y. Chu, A. Imamoglu, and M. D. Lukin, Laser cooling and real-time measurement of the nuclear spin environment of a solid-state qubit, Nature (London) **478**, 497 (2011).
[54] M. Issler, E. M. Kessler, G. Giedke, S. Yelin, I. Cirac, M. D. Lukin, and A. Imamoglu, Nuclear spin cooling using overhauser-field selective coherent population trapping, Phys. Rev. Lett. **105**, 267202 (2010).
[55] I. B. W. Harris, C. P. Michaels, K. C. Chen, R. A. Parker, M. Titze, J. A. Martinez, M. Sutula, I. R. Christen, A. M. Stramma, W. Roth, C. M. Purser, M. H. Appel, C. Li, M. E. Trusheim, N. L. Palmer, M. L. Markham, E. S. Bielejec, M. Atature, and D. Englund, Hyperfine spectroscopy of isotopically engineered group-IV color centers in diamond, arXiv:2306.00164.
[56] P. Jamonneau, A. Dréau, G. Hétet, J. F. Roch, J. R. Maze, and V. Jacques, Room-temperature polarization of individual nuclear spins in diamond via anisotropic hyperfine coupling and coherent population trapping, Eur. Phys. J. D **76**, 228 (2022).
[57] R. A. Parker, J. A. Martínez, K. C. Chen, A. M. Stramma, I. B. Harris, C. P. Michaels, M. E. Trusheim, M. H. Appel, C. M. Purser, W. G. Roth, D. Englund, and M. Atatüre, Diamond nanophotonic interface with an optically accessible deterministic electronuclear spin register, arXiv:2305.18923.
[58] F. Poggiali, P. Cappellaro, and N. Fabbri, High-fidelity projective readout of a solid-state spin quantum register, Phys. Rev. B **95**, 195308 (2017).
[59] L. Robledo, L. Childress, H. Bernien, B. Hensen, P. F. A. Alkemade, and R. Hanson, Measurement of the excited-state transverse hyperfine coupling in NV centers via dynamic nuclear polarization, Nature (London) **477**, 574 (2011).
[60] H. H. Vallabhapurapu, J. P. Slack-Smith, V. K. Sewani, C. Adambukulam, A. Morello, J. J. Pla, and A. Laucht, Fast coherent control of a nitrogen-vacancy-center spin ensemble using a $KTaO_3$ dielectric resonator at cryogenic temperatures, Phys. Rev. Appl. **16**, 044051 (2021).
[61] P. Neumann, J. Beck, M. Steiner, F. Rempp, H. Fedder, P. R. Hemmer, J. Wrachtrup, and F. Jelezko, Single-shot readout of a single nuclear spin, Science **329**, 542 (2010).
[62] H. H. Vallabhapurapu, C. Adambukulam, A. Saraiva, and A. Laucht, Indirect control of the $^{29}SiV^-$ nuclear spin in diamond, Phys. Rev. B **105**, 205435 (2022).
[63] Y. Wang, Z. Hu, B. C. Sanders, and S. Kais, Qudits and high-dimensional quantum computing, Front. Phys. **8** (2020).